Hyperfine Interact (2017) 238:82
https://doi.org/10.1007/s10751-017-1452-4

Nuclear inelastic scattering at the diiron center of ribonucleotide reductase from *Escherichia coli*

J. Marx[1] · V. Srinivas[2] · I. Faus[1] · H. Auerbach[1] · L. Scherthan[1] · K. Jenni[1] · A. I. Chumakov[3] · R. Rüffer[3] · M. Högbom[2] · M. Haumann[4] · V. Schünemann[1]

Abstract The enzyme ribonucleotide reductase R2 catalyzes an important step in the synthesis of the building blocks of DNA, and harbors a dinuclear iron center required for activity. Not only the iron valence states but also the protonation of the iron ligands govern the enzymatic activity of the enzyme. We have performed Nuclear Inelastic Scattering (NIS) experiments on the ^{57}Fe reconstituted ribonucleotide reductase R2 subunit from *Escherichia coli* (*Ec*R2a). Accompanying Mössbauer spectroscopic investigations show that the partial density of vibrational states (pDOS) of the ^{57}Fe reconstituted *Ec*R2a sample contained contributions from both ^{57}Fe-*Ec*R2a protein as well as unspecifically bound ^{57}Fe. Subtraction of a featureless pDOS as obtained from protein-coated iron oxide particles allowed modeling of the contribution of non-specifically bound iron and thus the pDOS of ^{57}Fe-*Ec*R2a could be obtained. Quantum-mechanics/molecular-mechanics (QM/MM) calculations of the whole ^{57}Fe-*Ec*R2a protein with variations of the cofactor protonation were performed in order to assign characteristic bands to their corresponding molecular vibrational modes.

Keywords Nuclear inelastic scattering · Ribonucleotide reductase R2 subunit · Density functional theory

This article is part of the Topical Collection on *Proceedings of the International Conference on the Applications of the Mössbauer Effect (ICAME 2017), Saint-Petersburg, Russia, 3–8 September 2017*
Edited by Valentin Semenov

✉ J. Marx
jmarx@physik.uni-kl.de

1 Department of Physics, University of Kaiserslautern, Kaiserslautern, Germany

2 Department of Biochemistry and Biophysics, Stockholm University, Stockholm, Sweden

3 Nuclear Resonance Group, European Synchrotron Radiation Facility, Grenoble, France

4 Department of Physics, Free University of Berlin, Berlin, Germany

Published online: 23 October 2017

1 Introduction

Ribonucleotide reductase (RNR) enzymes catalyze the formation of deoxyribonucleotides from ribonucleotides in the synthesis of DNA [1]. Class I RNR consists of two proteins, R1 and R2. One of the best known proteins of the R2 Ia class stems from *Escherichia coli (Ec*R2a). A prominent feature of this protein is a stable tyrosyl radical in the R2 unit close to the diiron center [2]. The reaction mechanism proposed by Mao et al. [3] involves the generation of a thiyl radical in the R1 subunit, which ultimately carries out the reduction of ribonucleotides [4], by means of a long-range proton-coupled electron transfer. The proteins of the R2a class carry a diiron cofactor. Its two iron ions may differ with respect to the coordination sphere [5]: In the structure at highest available resolution (∼1.4 Å), site 1 is 5-coordinate whereas site 2 has a 6-fold coordination [6, 7]. Both iron ions are shown to be in a Fe^{III} high spin (HS) state [5].

2 Materials and methods

Protein expression and reconstitution was performed after the procedure published in [7], $^{57}FeSO_4$ was used for iron reconstitution.

Nuclear Inelastic Resonant Scattering (NIS) [8] data were recorded at the ID 18 nuclear resonance beamline at ESRF (Grenoble) under experiment number LS-2422. The beamline was operated in 16 bunch mode. The data were recorded within an energy range of −20 to +100 meV from the elastic scattering line with a step size of 0.2 meV. The measuring time per scan was 1 second/channel with 560 channels. The shown pDOS data were obtained from the positive energy region of 12 scans, and a binning over a range of 0.5 meV was applied to improve the statistics. The elastic peak was subtracted from the data from −2 to 2 meV. Analysis of the NIS data was performed according to published procedures [9]. Mössbauer spectroscopy was done at liquid nitrogen temperature (77 K) in an OptistatDN Mössbauer Cryostat (Oxford Instruments) with a conventional Mössbauer spectrometer using constant acceleration mode. The spectral components were determined by performing least-mean-squares fit analysis using Lorentzian doublets. Mössbauer spectra with applied external fields were recorded in a setup as described in [10, 11], including a closed-cycle helium cryostat (Cryo Industries of America, Inc.) equipped with a superconducting magnet with a maximal field of 5 T, oriented parallel to the γ-radiation. The spectra were analyzed with WMOSS4f [12] using the spin Hamiltonian formalism [13, 14]. All Mössbauer parameters are quoted relative to α-iron foil at room temperature.

QM/MM Calculations were done with Gaussian 09, Rev. D. [15], using the ONIOM [15] method. The starting geometry was the X-ray crystal structure with the PDB ID 1MXR [16]. Hydrogens were added by the automatic algorithm included in GaussView 5.0 [17], except for the μ-oxo bridge and the terminal oxygen containing ligand at site 1, for which the hydrogens were added manually using GaussView. The model included a model layer treated at DFT level with the B3LYP hybrid functional [18] and the split-valence double zeta CEP-31G [19] basis set. The whole protein was treated with molecular mechanics using the universal force field (UFF) [20]. Geometry optimization with a convergence limit of 10^{-8} Hartree and an ultrafine integration grid was done, followed by a frequency calculation based on normal mode analysis. The simulated partial density of vibrational states of ^{57}Fe was obtained by using the nisspec2 program [21]. Analysis of the vibrational modes was done with GaussView 5.0.

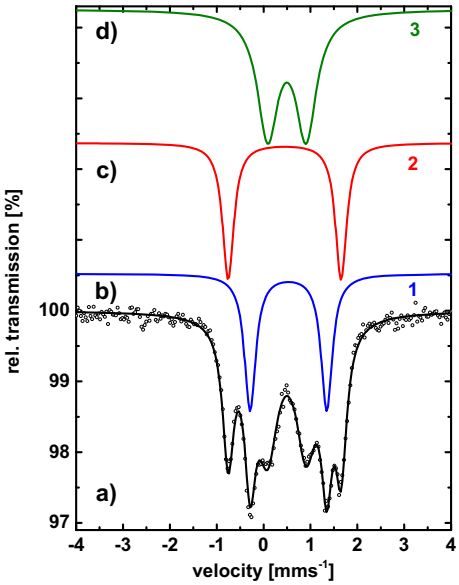

Fig. 1 Mössbauer spectra of the *Ec*R2a sample (**a**, shown as dots), obtained at 77 K. Simulated subspectra for component 1 (blue, **b**), 2 (red, **c**) and 3 (green, **d**) are shown as lines above the experimental spectrum. The sum of the simulations is shown as a black line in **a**

3 Results and discussion

Figure 1 shows the Mössbauer spectrum of the *Ec*R2a sample measured at 77 K. The simulation (black line) includes three components: Component 1 (blue line in Fig. 1b) has an isomer shift of $\delta_1 = 0.53$ mms^{-1} and a quadrupole splitting of $\Delta E_{Q1} = 1.63$ mms^{-1}, component 2 (Fig. 1c, red line) has $\delta_2 = 0.45$ mms^{-1} and $\Delta E_{Q2} = 2.41$ mms^{-1}. The linewidth is $\Gamma_{1,2} = 0.30$ mms^{-1} for both components. These values correspond to the two iron sites of the oxidized *Ec*R2a as reported by Lynch et al. [5] and Bollinger et al. [22]. While the isomer shifts represent typical values for high spin Fe^{III}, the quadrupole splittings have a higher value due to the short iron-oxo distances of the μ-oxo bridge [23]. Component 3 (green line in Fig. 1d) has $\delta_3 = 0.50$ mms^{-1} and $\Delta E_{Q3} = 0.82$ mms^{-1}, values which are also typical for Fe^{III}-HS. ΔE_{Q3} is not in the range for μ-oxo-bridged iron, nor is it in the range of any reaction intermediate of *Ec*R2a [4, 22, 24, 25]. The linewidth $\Gamma_3 = 0.53$ mms^{-1}) is also significantly larger than the linewidth of the other two components, indicating that this is an iron species showing relaxational broadening [26]. Such iron species showing fast relaxation can form in a protein sample during the ^{57}Fe reconstitution due to excess iron, which may unspecifically bind to the protein surface, where it forms iron-oxide and -hydroxide species after oxidation [27]. Based on the relative surface areas and assuming a similar Lamb-Mössbauer factor for all three components, it can be concluded that 45% of the iron present in the sample was not coordinated in the *Ec*R2a diiron cluster.

The Mössbauer spectrum of the sample measured at 4.2 K in an external magnetic field of 5 T oriented parallel to the γ radiation is shown in Fig. 2. It gives further evidence on the third component being a superparamagnetic species, as the spectrum contains a broad, magnetically split background. The diamagnetic components (1 and 2 in Fig. 2, shown as blue and red lines above the spectrum) were simulated with the parameters of the two sites of *Ec*R2a as obtained from the 77 K spectrum (Fig. 1) and η taken from [5] (Table 1).

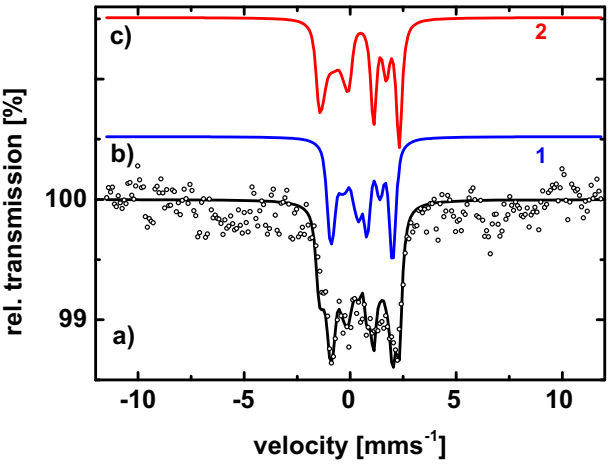

Fig. 2 Mössbauer spectra of the *Ec*R2a sample (**a**, shown as dots), obtained at 4.2 K in an external magnetic field of 5 T oriented parallel to the γ-ray. Simulated subspectra for component 1 (blue, **b**) and 2 (red, **c**) are shown as lines above the experimental spectrum. The sum of the simulations is shown as a black line in **a**). Component 3 from Fig. 1 was not included in the simulation as it was broad and featureless

Table 1 Parameters obtained from the Mössbauer spectra for the components of the *Ec*R2a sample

	Component 1	Component 2	Component 3
δ (mms^{-1})	0.53 ± 0.02	0.45 ± 0.02	0.50 ± 0.02
ΔE_Q (mms^{-1})	1.63 ± 0.03	2.41 ± 0.03	0.82 ± 0.04
η (taken from [5])	0.6	0.2	–
Γ (mms^{-1})	0.29 ± 0.02 (0T)/ 0.40 ± 0.10 (5T)	0.29 ± 0.02 (0T)/ 0.40 ± 0.10 (5T)	0.53 ± 0.02 (0T)
rel. area (%)	27.4 ± 1.5	27.4 ± 1.5	45.2 ± 1.5

The simulated spectra of these two components are in good agreement with the experimental spectrum, leading to the conclusion that they are indeed originating from the oxidized Fe^{III}/Fe^{III} cluster of *Ec*R2a, which has a diamagnetic ground state.

The partial density of (vibrational) states (pDOS) as derived from the NIS data of the *Ec*R2a sample is shown in Fig. 3a. Figure 3c shows a pDOS of BSA-iron oxide nanoparticles taken from [28]. This pDOS may serve as a model for the unspecifically bound iron oxide/hydroxide form which is represented by component 3 in the Mössbauer spectra. Keeping in mind that areas of the experimental pDOS shown in Fig. 3a and c are normalized to unity and that Mössbauer spectroscopy shows that there is 45% unspecifically bound iron in the *Ec*R2a sample we have obtained the protein *Ec*R2a pDOS by subtracting the data shown in Fig. 3c) from the data shown in Fig. 3a) using a scaling factor of 0.45. The resulting *Ec*R2a pDOS -again scaled to unity- is shown in Fig. 3b).

The theoretical pDOS obtained from a QM/MM-DFT simulation is shown as a blue line in Fig. 3d. For the further discussion, four spectral regions of the pDOS will be considered: Region 1 from 0–125 cm^{-1} showing no distinct features, region 2 from 125–250 cm^{-1}, region 3 from 250–450 cm^{-1} and region 4 starting at 450 cm^{-1}.

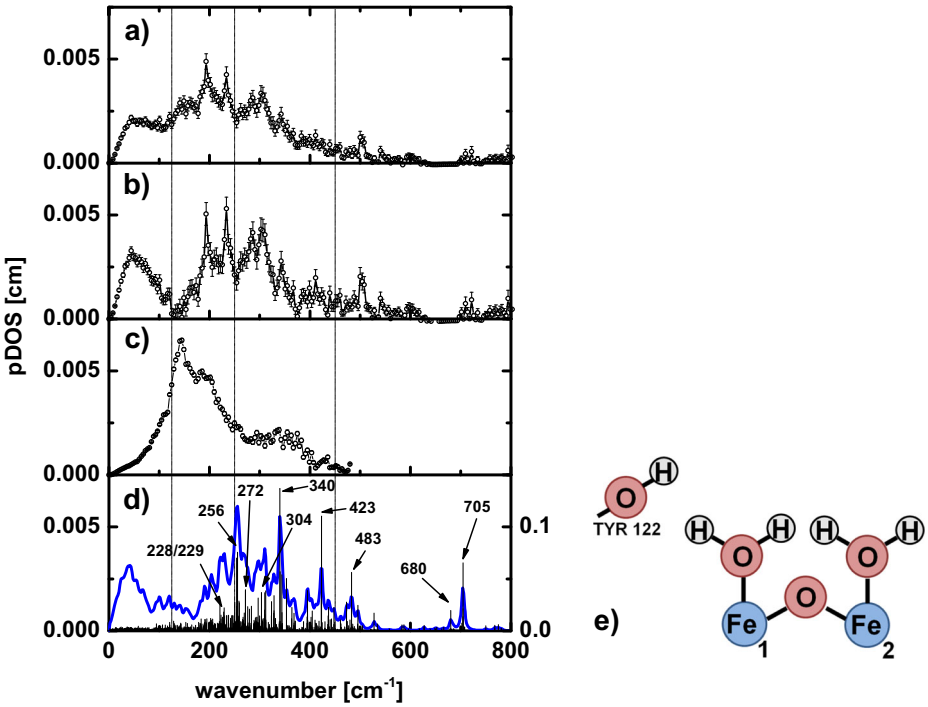

Fig. 3 **a** Experimental pDOS of the *Ec*R2a sample containing the diiron cofactor and unspecifically bond iron **b** Experimental pDOS of *Ec*R2a protein resulting from subtracting a model pDOS from BSA-coated iron-oxide nanoparticles scaled by a factor of 0.45 from the data shown in (**a**). Details: see text. **c** Esperimental pDOS of BSA-coated iron-oxide nanoparticles, taken from [28] used as a model for the non-specifically bound iron. **d** Simulated pDOS obtained from DFT calculations for the model with protonated Tyr 122. The black bars represent the normalized means square displacement of the iron, the modes which are discussed in the text are marked with arrows, labels refer to the energy of the modes in [cm^{-1}]. **e** Schematic representation of the refined protonation model for the diiron cluster

For a better comparison the bands and modes discussed in the text are given as an overview in Table 2. The experimental pDOS of the *Ec*R2a (Fig. 3a) shows a generally higher intensity in the low energy region below 250 cm^{-1} than the simulated pDOS (Fig. 3d), which was obtained using the x-ray crystal structure with a refined model for the diiron cofactor as shown in Fig. 3e. After subtraction of the model pDOS for unspecifically bound iron (Fig. 3c), the band is distinctly reduced at 142 cm^{-1} (Fig. 3b). Together with the results obtained via Mössbauer spectroscopy, it can be concluded that this band originated from the unspecific iron impurity in the sample. The enhanced intensity in regions 1 and 2 could be successfully removed by subtracting a model pDOS, leading to a pDOS that now mostly contains information on the oxidized diiron cofactor of *Ec*R2a. The further discussion will therefore concentrate on the *Ec*R2a pDOS displayed in Fig. 3b.

In region 2, the experimental pDOS of *Ec*R2a shows two intense bands at 194 and 234 cm^{-1}, whereas bands are found at 190 and 204 and 222/230 cm^{-1} in the simulated pDOS. Region 3 shows bands at 284, 302, 342, 394 cm^{-1} and 411 cm^{-1} in the experimental pDOS, whereas the simulated pDOS shows intense bands at 254, 298, 310, 340, 396, and 424 cm^{-1}. The region above 450 cm^{-1} the experimental pDOS shows bands at 458, 500,

Table 2 Comparison of band energies obtained from the experimental pDOS, from the calculated pDOS and of the most intense modes discussed in the text

Experimental bands (cm^{-1})	Calculated band maximum (most bands consist of several calculated modes) (cm^{-1})	Most intense modes (contributing to the simulated bands) (cm^{-1})
194	190	Not discussed
	204	
234	222/230	228/229
	254	256
284	298	272
302	310	304
342	340	340
394	396	Not discussed
411	424	423
458	–	–
500	474/482	483
	496	Not discussed
542	528	Not discussed
710	680	680
722	704	705

542, 710, and 722 cm^{-1}, compared to bands at 474, 482, 496, 528, 680, and 704 cm^{-1} in the simulated pDOS.

The normal mode calculation also gives information on the type of displacement of the iron in vibrational modes which e.g. include displacements of the whole cluster and/or specific iron-ligand modes like Fe-μO-stretch modes. At energies close to the experimental band at 234 cm^{-1}, displacements of both iron centers combined with in-plane rotations of the histidine residues could be identified. The calculated mode at 256 cm^{-1} does not correspond to a band in region 3, but is close to the intense experimentally observed band at 234 cm^{1} in region 2. It shows a displacement of the two iron centers opposite to each other. The closest calculated intense mode in the range of the experimental band at 286 cm^{-1} is at 272 cm^{-1}. It shows a displacement of both iron ions in opposition with Fe(1) in direction of the His 118/H_2O(2) axis and Fe(2) between Glu 238 and H_2O.

The calculated mode at 304 cm^{-1} is close to the experimental band found at 302 cm^{-1}. For this mode, both iron ions show an in-phase displacement with the μ-oxo oxygen moving in the opposite direction forming a Fe-O-Fe bending mode. In the energy range of the experimental band at 342 cm^{-1} the most intense calculated mode is at 340 cm^{-1} (Fig. 4f). It shows a displacement of both irons in opposite direction and a displacement of the μ-oxo oxygen perpendicular to the iron-iron axis. Both water ligands contribute with a displacement in the opposite direction of the iron displacements. The calculated mode at 423 cm^{-1} (Fig. 4i) is in the same energy range as the experimental band at 411 cm^{-1}. This mode is characterized by a Fe(1)-OH_2 stretch accompanied by an in-plane rotation of tyrosine 122. Tyr 122 is important for the catalytic activity of the R2a, as it is used to store a stable radical in the active form of R2a [2].

Above 450 cm^{-1} only few, but intense modes were calculated for the simulation. Modes were calculated at energies of 483, 680 and 705 cm^{-1}. The mode at 483 cm^{-1} is close to

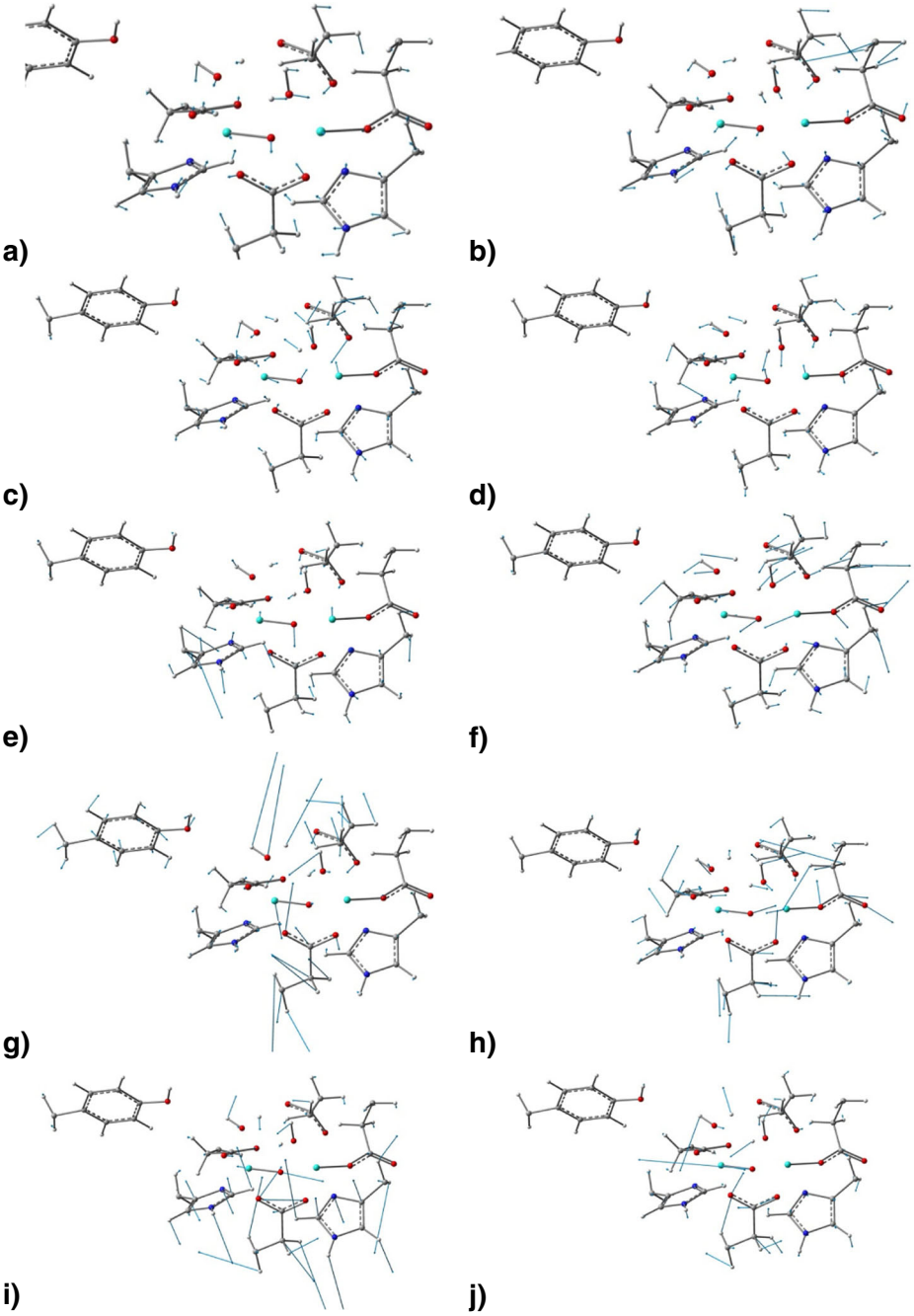

Fig. 4 Atom displacements for simulated modes at 228 (**a**), 229 (**b**), 256 (**c**), 272 (**d**), 304 (**e**), 340 (**f**), 423 (**g**), 483 (**h**), 680 (**i**) and 705 cm^{-1} (**j**). Iron atoms are colored in margenta, ogygen in red, nitrogen in blue, carbon in dark gray and protons in pale gray

the experimental band at 500 cm^{-1}, the modes at 680 and 705 cm^{-1} are close to the experimentally obtained bands at 710 and 722 cm^{-1}. All of these modes show an asymmetric Fe-O-Fe-stretch character. A prominent waving of both histidine ligands can be seen for the mode at 680 cm^{-1} lower energy. Sjöberg et al. assigned the asymmetric stretch modes to a band located at 756 cm^{-1} in room-temperature Raman spectra [29]. Compared to the highest experimentally observed band at 722 cm^{-1} in NIS, this would be a shift of 36 cm^{-1} to higher wavenumbers. The exact position could not be determined by Sjöberg et al. due to an underlying band, but this shift is larger than the uncertainty in mode assignment.

According to [30] an Fe-O-stretch around 720 cm^{-1} corresponds to a Fe-O-Fe angle of 120°. The 756 cm^{-1} mode as reported by Raman spectroscopy [29] thus corresponds to a Fe-O-Fe angle of 130°. Since there is some spectral noise in the 700–800 cm^{-1} region in our *Ec*R2a pDOS (Fig. 3b) and also in the Raman data of ref [29] it is reasonable to assume that the 756 cm^{-1} mode is not intense enough to be observed by NIS and that the diferric iron center of *Ec*R2a possibly has two conformations in frozen solution.

Short Fe-O distances are also expected for proteins of the R2c subgroup, which most probably are bridged by a μ-oxo and a μ-hydroxo bridge in their Mn(IV)Fe(III) form [31]. However, in a NIS study by Kwak et al. [32] no features at energies higher than 400 cm^{-1} could be found. In a previous NIS study on *Gk*R2lox, which most probably has a μ-hydroxo bridge and no μ-oxo bridge, no features at energies higher than 550 cm^{-1} could be found experimentally for both, the Mn(III)Fe(III) and the Fe(III)Fe(III) form [33]. This is in accordance with the generally longer Fe-O distances in μ-hydroxo bridges and further emphasizes the importance of this energy region as a marker region for vibrations of iron and oxygen in short μ-oxo bridges. As our data clearly show (Fig. 3a,b), we do have features in this spectral region in *Ec*R2a, and our calculations (Fig. 4g–j) show corresponding modes with a displacement of primarily Fe(1), which is replaced by Mn in the R2c and R2lox in their MnFe form. This is partly in accordance with the theoretical findings by Kwak et al. [32], although the theoretical calculations shown therein unfortunately don't include the energy range above 650 cm^{-1} where the asymmetric Fe-O-Fe stretching bands could be found in our study both theoretically and experimentally.

In conclusion we obtained the pDOS of *Ec*R2a protein containing the oxidized cofactor with two ferric iron ions and unspecifically bound surplus iron. Mössbauer spectroscopy was used for quantitative discrimination between both iron species. We were able to show that the unspecific iron could be subtracted from the experimental pDOS by using a model pDOS of protein-coated iron oxide nanoparticles, leading to a pDOS that agrees well with a theoretical pDOS for *Ec*R2a obtained via ONIOM-DFT calculations. Normal mode analysis showed a mode at 423 cm^{-1} where the catalytically important Tyr 122 was displaced along with the water ligand at site 1. From our experimental and theoretical findings we conclude that Fe-O-Fe stretching marker bands characteristic for R2a proteins with diiron cofactors with a short μ-oxo-bridge may be found in the energy range above 650 cm^{-1}.

Acknowledgements This work has been supported by the German Federal Ministry of Education and Research and the Swedish Research Council via the German-Swedish Röntgen-Ångström-Cluster.

References

1. Högbom, M.: Metal use in ribonucleotide reductase R2, di-iron, di-manganese and heterodinuclear—an intricate bioinorganic workaround to use different metals for the same reaction. Metallomics **3**, 110–120 (2011)

2. Sahlin, M., Graeslund, A., Petersson, L., Ehrenberg, A., Sjoeberg, B.M.: Reduced forms of the iron-containing small subunit of ribonucleotide reductase from Escherichia coli. Biochemistry **28**(6), 2618–2625 (1989)
3. Mao, S.S., Yu, G.X., Chalfoun, D., Stubbe, J.: Characterization of C439SR1, a mutant of Escherichia coli ribonucleotide diphosphate reductase: evidence that C439 is a residue essential for nucleotide reduction and C439SR1 is a protein possessing novel thioredoxin-like activity. Biochemistry **31**(40), 9752–9759 (1992)
4. Sturgeon, B.E., Doug Burdi, D., Chen, S., Huynh, B.-H., Edmondson, D.E., Stubbe, J., Hoffman, B.M.: Reconsideration of X, the Diiron Intermediate Formed during Cofactor Assembly in E. coli Ribonucleotide Reductase. J. Am. Chem. Soc. **118**(32), 7551–7557 (1996)
5. Lynch, J.B., Juarez-Garcia, C., Münck, E., Que, L.J.: Mössbauer and EPR studies of the binuclear iron center in ribonucleotide reductase from Escherichia coli. J. Biol. Chem. **264**(14), 8091–8096 (1989)
6. Nordlund, P., Sjöberg, B.-M., Eklund, H.: Three-dimensional structure of the free radical protein of ribonucleotide reductase. Nature **345**, 593–598 (1990)
7. Högbom, M., Galander, M., Andersson, M., Kolberg, M., Hofbauer, W., Lassmann, G., Nordlund, P., Lendzian, F.: Displacement of the tyrosyl radical cofactor in ribonucleotide reductase obtained by single-crystal high-field EPR and 1.4-Å x-ray data, pdb ID 1MXR. Proc. Natl. Acad. Sci. USA **100**(6), 3209–3214 (2003)
8. Sjöberg, B.-M., Hahne, S., Karlsson, M., Jörnvall, H., Göransson, M., Uhlin, B.E.: Overproduction and purification of the B2 subunit of ribonucleotide reductase from Escherichia coli. J. Biol. Chem. **261**, 5658–5662 (1986)
9. Sturhahn, W., Toellner, T.S., Alp, E.E., Zhang, X., Ando, M., Yoda, Y., Kikuta, S., Seto, M., Kimball, C.W., Dabrowski, B.: Phonon density of states measured by inelastic nuclear resonant scattering. Phys. Rev. Lett. **74**(19), 3832–3835 (1995)
10. Kohn, V.G., Chumakov, A.I.: DOS: Evaluation of phonon density of states from nuclear inelastic scattering. Hyperfine Interact. **125**, 205–221 (2000)
11. Janoschka, A., Svenconis, G., Schünemann, V.: A closed cycle-cryostat for high-field Mössbauer spectroscopy. J. Phys. Conf. Ser. **217**, 012005 (2010)
12. Bauer, T.O., Graf, D., Lamparter, T., Schünemann, V.: Characterization of the photolyase-like iron sulfurprotein PhrB from Agrobacterium tumefaciens by Mössbauer spectroscopy. Hyperfine Interact. **226**, 445–449 (2014)
13. Prisecaru, I.: WMOSS4 Mössbauer Spectral Analysis Software, 2009–2016. [online: http://www.wmoss.org]
14. Trautwein, A.X., Bill, E., Bominaar, E.L., Winkler, H.: Iron-containing proteins and related analogs—complementary Mössbauer, EPR and magnetic susceptibility studies. In: Structure and bonding, vol. 78. Springer, Berlin (1991)
15. Schünemann, V., Winkler, H.: Structure and dynamics of biomolecules studied by Mössbauer spectroscopy. Rep. Prog. Phys. **63**, 263–353 (2000)
16. Frisch, M.J., Trucks, G.W., Schlegel, H.B., Scuseria, G.E., Robb, M.A., Cheeseman, J.R., Scalmani, G., Barone, V., Mennucci, B., Petersson, G.A., Nakatsuji, H., Caricato, M., Li, X., Hratchian, H.P., Izmaylov, A.F., Bloino, J., Zheng, G., Sonnenberg, J.L., Hada, M., Ehara, M., Toyota, K., Fukuda, R.: Gaussian 09, Revision D.01. Wallingford (2009)
17. Dennington, R., Keith, T., Millam, J.: GaussView, Version 5 (2009)
18. Becke, A.D.: Density-functional thermochemistry. III. The role of exact exchange. J. Chem. Phys. **98**(7), 5648–5652 (1993)
19. Stevens, W.J., Basch, H., Krauss, M.: Compact effective potentials and efficient shared-exponent basis sets for the first- and second-row atoms. J. Chem. Phys. **81**(12), 6026–6033 (1984)
20. Rappe, A.K., Casewit, C.J., Colwell, K.S., Goddard, W.A., Skiff, W.M.: UFF, a full periodic table force field for molecular mechanics and molecular dynamics simulations. J. Am. Chem. Soc. **114**(25), 10024–10035 (1992)
21. Paulsen, H., Winkler, H., Trautwein, A.X., Grünstreudel, H., Rusanov, V., Toftlund, H.: Measurement and simulation of nuclear inelastic-scattering spectra of molecular crystals. Phys. Revi. B **59**(2), 975–984 (1999)
22. Bollinger, J.M. Jr., Tong, W.H., Ravi, N., Huynh, B.H., Edmondson, D.E., Stubbe, J.: Mechanism of assembly of the tyrosyl radical-diiron (III) cofactor of E. coli ribonucleotide reductase: 1. Mössbauer characterization of the diferric radical precursor. J. Am. Chem. Soc. **116**, 8015–8023 (1994)
23. Kurtz, D.M.J.: Oxo- and hydroxo-bridged diiron complexes: a chemical perspective on a biological unit. Chem. Rev. **90**, 585–606 (1990)
24. Ravi, N., Bollinger, J.M.J., Huyhn, B.H., Edmondson, D.E., Stubbe, J.: Mechanism of assembly of the tyrosyl radical-diiron(III) cofactor of E. Coli ribonucleotide reductase. 1. Mössbauer characterization of the diferric radical precursor. J. Am. Chem. Soc. **116**, 8007–8014 (1994)

25. Dong, Y., Que, L.J., Kauffmann, K., Münck, E.: An exchange-coupled complex with localized high-spin Fe^{IV} and Fe^{III} sites of relevance to cluster X of Escherichia coli ribonucleotide reductase. J. Am. Chem. Soc. **117**, 11377–11378 (1995)
26. Mørup, S.: Paramagnetic and Superparamagnetic Relaxation Phenomena Studied by Mössbauer Spectroscopy. Polyteknisk Forlag, Lyngby (1981)
27. Cornell, R.M., Schwertmann, U.: The Iron Oxides, 2nd edn. Wiley-VCH, Weinheim (2002)
28. Marx, J., Huang, H., Faus, I., Rackwitz, S., Wolny, J.A., Schlage, K., Ulber, R., Wille, H.-C., Schünemann, V.: Simultaneous characterization of protein coated iron oxide nanoparticles with nuclear inelastic scattering and atomic force microscopy. Hyperfine Interact. **226**, 661–665 (2014)
29. Sjoberg, B.-M., Sanders-Loehr, J., Loehr, T.M.: Identification of a hydroxide ligand at the iron center of ribonucleotide reductase by resonance raman spectroscopy. Biochemistry **26**, 4242–4247 (1987)
30. Sanders-Loehr, J., Wheeler, W.D., Shiemke, A.K., Averill, B.A., Loehr, T.M.: Electronic and Raman spectroscopic properties of oxo-bridged dinuclear iron centers in proteins and model compounds. J. Am. Chem. Soc. **111**, 8084–8093 (1989)
31. Younker, J.M., Krest, C.M., Jiang, W., Krebs, C., Bollinger, J.M.J., Green, M.T.: Structural analysis of the Mn(IV)/Fe(III) cofactor of chlamydia trachomatis ribonucleotide reductase by extended X-ray absorption fine structure spectroscopy and density functional theory calculations. J. Am. Chem. Soc. **130**(45), 15022–15027 (2008)
32. Kwak, Y., Wei, Y., Dassama, L.M.K., Park, K., Bell, C.B., Liu, L.V., Wong, S.D., Saito, M., Kobayashi, Y., Kitao, S., Seto, M., Yoda, Y., Alp, E., Zhao, J., Bollinger, J.-M.J., Krebs, C., Solomon, E.I.: Geometric and electronic structure of the Mn(IV)Fe(III) cofactor in class Ic ribonucleotide reductase: correlation to the class Ia binuclear non-heme iron enzyme. J. Am. Chem. Soc. **135**, 17573–17584 (2013)
33. Kositzki, R., Mebs, S., Marx, J., Griese, J.J., Schuth, N., Högbom, M., Schünemann, V., Haumann, M.: Protonation state of MnFe and FeFe cofactors in a ligand-binding oxidase revealed by X-ray absorption, emission, and vibrational spectroscopy and QM/MM calculations. Inorg. Chem. **55**(19), 9869–9885 (2016)